Mondal, A.K.; Kesavan, A.R.; Reddy, B.R.K.; Dieringa, H.; Kumar, S.:
Correlation of microstructure and creep behaviour of MRI230D Mg alloy developed by two different casting technologies
In: Materials Science and Engineering A (2015) Elsevier

DOI: 10.1016/j.msea.2015.02.037

Correlation of microstructure and creep behaviour of MRI230D Mg alloy developed by two different casting technologies

A. K. Mondal[a,*], Arjun Rajiv Kesavan[a], B. Ravi Kiran Reddy[a], Hajo Dieringa[b] and S. Kumar[c]

[a]Department of Metallurgical and Materials Engineering, National Institute of Technology, Rourkela-769008, India.

[b]Magnesium Innovation Centre- MagIC, Institute for Materials Research, Helmholtz-Zentrum Geesthacht, Max-Planck-Straße 1, 21502 Geesthacht, Germany.

[c]Department of Materials Engineering, Indian Institute of Science, Bangalore-560012, India.

Abstract

The relationship between the as-cast microstructure and creep behaviour of the heat-resistant MRI230D Mg alloy produced by two different casting technologies is investigated. The alloy in both ingot-casting (IC) and high pressure die-casting (HPDC) conditions consists of α-Mg, C36 ($(Mg,Al)_2Ca$), Al-Mn and Sn-Mg-Ca rich phases. However, the HPDC alloy resulted in relatively finer grain size and higher volume fraction of finer, denser network of eutectic C36 phase in the as-cast microstructure as compared to that of the IC alloy. The superior creep resistance exhibited by the HPDC alloy at all the stress levels and temperatures employed in the present investigation was attributed to the more effective dispersion strengthening effect caused by the presence of finer and denser network of the C36 phase. The increased amount of the eutectic C36 phase was the only change observed in the microstructures of both alloys following creep tests.

*Corresponding author. Tel.: +91 661 246 2571; fax: +91 661 246 2551.

E-mail addresses: mondala@nitrkl.ac.in; ashok.mondal@gmail.com (A. K. Mondal).

Keywords: A. Strain measurement; A. X-ray diffraction; B. Magnesium alloy; C. Casting; D. Plasticity; D. Precipitation

1. Introduction

Recently the emphasis given by automobile manufacturers in prioritising fuel conservation and emission quality on par with performance, has led to the concept of weight reduction. Magnesium (Mg) alloys are considered to be the most suitable alternative as structural materials in automobiles owing to their high specific strength, good dimensional stability, high damping capacity, excellent machinability and appreciable casting properties [1].

Powertrain applications of automobile require Mg alloys which can sustain high temperature. The major limitation of application of Mg alloy in the automobile industry is poor creep resistance being a significant factor above 100^{o}C owing to the presence of thermally unstable β-$Mg_{17}Al_{12}$ phase [2]. This makes it inappropriate for powertrain applications where service temperature and stress are in the range of 150-300ºC and 50-70 MPa, respectively [3,4]. Attempts were made to improve creep resistance of the Mg-Al based alloys by introducing thermally stable intermetallics through the addition of different alloying elements like RE, Ca, Si, Sn, Sb and so on [5-7]. Among these the Ca containing Mg-Al based alloys are the most economic and exhibited promising properties [6,7]. MRI230D is a Ca containing alloy developed by Dead-Sea Magnesium and Volkswagen AG for its commercial usage to enhance the sphere of utility overcoming the limitations of popular alloy like AZ91 and it is suitable for application up to 190^{o}C [8].

Mg alloys are mostly used in as-cast condition and the casting condition plays a crucial role in the resulting properties. Factors such as porosity, solidification rate, grain size, volume

fraction and morphology of intermetallic phases, degree of solute supersaturation as well as various strengthening mechanisms affect creep and other mechanical properties of Mg alloys. Gutman [9] investigated the influence of casting parameters on creep and strength of AZ9lD alloy and established that precipitation of β phase improved creep resistance of permanent mold cast alloy. For die-cast alloy, creep was controlled by the extent of micro and macro porosity. Spiragarelli et al. [10] reviewed the literature on creep behaviour of AZ91 alloy produced by die-casting, ingot-casting and thixoforming and concluded that the creep behaviour of the alloy depends on grain size and intragranular precipitates interacting with dislocations. Caceres et al. [11] reported variation in tensile properties of AZ91 alloy fabricated by sand-castings with varying cooling rates. Zhu et al. [12] investigated the creep properties of Mg-Al-Ca alloy produced by die-casting, squeeze-casting and ingot-casting. The best and the worst creep resistance were exhibited by the squeeze-cast and the die-cast alloys whereas the ingot-cast alloy exhibited the intermediate creep resistance. Han et al. [13] observed that the nanoscale indentation creep behaviour of AC52 alloy increased with an increase in cooling rate. Srinivasan et al. [14] investigated the effect of intermetallic phases on the creep behaviour of AZ91 alloy and observed that the intermetallic phases strengthen the grain boundaries against sliding and reduce the possibility of void formation during creep. Ferri et al. [15] investigated the effect of solidification rates on mechanical properties of ZAXLa05413 alloy and observed a direct relationship between grain size and secondary dendritic arm spacing with improved mechanical properties. Zheng et al. [16] reported superior creep and other mechanical properties of the Mg-3Sm-0.5Zn-0.4Zr (wt.%) alloy in die-cast condition. Kim et al. [17] too stated that the die-cast alloy with relatively higher volume fraction of Mg_2Sn and CaMgSn phases exhibited higher creep resistance as compared to the ingot-cast alloy in the Mg-4Al-2Sn alloy containing Ca. Bai et al. [18] too observed the

difference in tensile and creep properties owing to the difference in casting conditions in the Mg-4Al-(1-4) La alloy.

The conclusion arising out of the afore-mentioned review points out that creep and other mechanical properties of Mg alloys vary significantly with casting technologies. Therefore, it is worth examining its effect on creep behaviour of the promising creep-resistant MRI230D Mg alloy developed for automobile powertrain applications, as there is paucity in the literature. In the present investigation an attempt has been made to apprehend the relationship between the microstructure and creep behaviour of the MRI230D alloy in different casting conditions (i.e., ingot-casting (IC) and high pressure die-casting (HPDC)) in order to substantiate the better casting technology for mass production.

2. Experimental procedure

The nominal chemical composition of the MRI230D alloy is shown in Table 1. The HPDC alloy was cast into cylindrical rod having 19 mm diameter and 179 mm length using a cold chamber high pressure die-casting machine (Model: FRECH DAK 450-54RC). The melt temperature was 690°C and the pressure during solidification was 300 bar. For gravity casting the melting was carried out in an electrical resistance furnace using stainless steel crucible. The melt temperature was 690°C and it was poured into a steel mould preheated to 250°C. During melting solid flux provided by FOSECO Industries Limited were used to protect the melt from oxidation. A mixture of SF_6 (0.5 vol.%) and Ar (99.5 vol.%) was purged to protect the melt during pouring. The IC alloy was cast into rectangular block with dimension of 350 mm (L)*125 mm (W)*60 mm (H) using conventional gravity casting. The specimens for creep testing having 6 mm diameter and 15 mm length were machined from the respective castings by spark erosion technique. All the creep tests were carried out in

compression using a lever arm (10:1) creep set-up (Model: ATS 2330) in the stress range of 60 to 120 MPa and at temperatures of 175ºC and 200ºC. The specimens for microstructural investigation were prepared by standard metallographic techniques. Etching of the specimens was carried out using a solution of 100 ml ethanol, 10 ml acetic acid, 6 ml picric acid and 20 ml of distilled water. Microstructural observation of the alloys were carried out using optical microscopy (OM) and field emission scanning electron microscopy (FESEM) (Model: FEI Sirion XL30) armed with an energy dispersive X-ray spectroscopy (EDS). The phases present in the alloy in both casting conditions were identified by X-ray diffraction (XRD) using CuK_{α} radiation (λ=1.541Å).

3. Results and discussion

3.1 As-cast microstructure

Fig. 1 shows the XRD patterns obtained from the as-cast MRI230D alloy in both casting conditions. It is evident from the figure that the alloy in both casting conditions consists of primary Mg (α-Mg) peak and the peak corresponding to $(Mg,Al)_2Ca$ phase. The peak corresponding to β-$Mg_{17}Al_{12}$ phase was not present. Thus, the low melting point β-$Mg_{17}Al_{12}$ phase generally observed in Mg-Al alloys is completely suppressed with the addition of Ca in the present investigation, which is beneficial for creep resistance. Mondal et al. [19] too reported elimination of β phase in the Mg-Al alloy with addition of RE. Bai et al. [18] observed the suppression of β phase in the IC and HPDC Mg-4Al-(1-4)La alloy with increase of La as well.

Optical micrographs of the MRI230D alloy in two different casting conditions are shown in Fig. 2 (a&b). The alloy in both casting conditions consists of polygonal grains. However, it is obvious that the HPDC alloy exhibited relatively finer grain size as compared to that of the

IC alloy. The average grain size determined by linear intercept method was 35±1 μm and 8±0.5 μm for the IC and HPDC alloys, respectively.

The SEM micrographs of the MRI230D alloy in two different casting conditions are shown in Fig. 3 (a&b) and the magnified view of Fig. 3(b) is shown in Fig. 3(c). EDS analysis carried out at the grain interior of the micrograph shown in Fig. 3(c) exhibited an average composition of 96.50±0.67 Mg, 2.70±0.64 Al, 0.30±0.14 Ca, 0.19±0.05 Sr, 0.17±0.03 Sn and 0.20±0.06 Mn (at.%), which corresponds to α-Mg. Similarly, EDS analysis from the bright lamellar phase present along the grain boundaries and triple points revealed an average composition of 38.7±4.2 Mg, 45.2±7.3 Al and 15.8±1.8 Ca (at.%). EDS analysis carried out by Terada et al. [20] on the grain boundary eutectic phase exhibited an average composition of 24.7 Mg, 56.9 Al and 18.0 Ca (at.%) and they have reported it as C36 ($(Mg, Al)_2Ca$) phase in the litertaure. Therefore, the grain boundary phase is probably be the C36 phase as marked by the arrows in Fig. 3(c). In addition, a few globular Al-Mn rich particles (shown by arrows in Fig. 3(c)) were also observed and EDS analysis exhibited an average composition of 52.3±8.6 Al, 39.6±2.3 Mn and 8.1±0.8 Mg (at.%). EDS analysis was also carried out from the IC specimen (marked by arrows in Fig. 3(a)) revealing the grain interior as α-Mg; the bright lamellar continuous eutectic phase present along the grain boundaries and triple points as C36 phase; and a few Al-Mn rich phase. In addition, a few irregular shaped Sn-Mg-Ca rich intermetallic particles were also observed in the alloy in both casting conditions (marked by arrows in Fig. 3(a&c)). Thus, the MRI230D alloy in both casting conditions confirms the existence of same phases i.e., α-Mg, C36, Al-Mn and Sn-Mg-Ca rich phases. The microstructures of the MRI230D alloy closely resembles to that of the HPDC AZ91 alloy. However, the eutectic phase is β-$Mg_{17}Al_{12}$ in HPDC AZ91 alloy, whereas, it is C36 ($(Mg,Al)_2Ca$) phase in MRI230D alloy [19].

The IC and HPDC alloys differed much on the following grounds. Firstly, the HPDC alloy exhibited finer grain size owing to the higher solidification rate as compared to the large grain size exhibited by IC alloy having lower solidification rate. The solidification rate associated with IC and HPDC is generally in the range of 10-20ºC/s and 100-120ºC/s, respectively [21]. The high degree of undercooling associated with the faster cooling rate following HPDC facilitates the formation of a large number of nuclei in the liquid Mg alloy. However, the sluggish diffusion rate at the corresponding temperature leading to low growth rate resulted in microstructural refinement [22]. Secondly, the caluclated average volume fraction of the grain boundary phase in the IC alloy (i.e., 9.1±0.4%) was lower as compared to that observed in the HPDC alloy (i.e., 12.8±3.2%). Han et al. [13] observed that the calculated volume fraction of the grain boundary eutectic phase increases with increase in cooling rate in the AC52 alloy. Faster cooling rate deviate the solidus line from its equilibrium position and enable the HPDC specimen to have a large amount of eutectic phase along the grain boundaries [23]. Another noteworthy dissimilarity observed was the difference in morphology of the second phase (i.e., C36 phase) precipitates. The observed second phase was finer and constituted a denser network along the grain boundaries and the triple points owing to the rapid solidification rate in the HPDC alloy, whereas, it was relatively coarser in the IC alloy. The IC alloy allows sufficient time for growth of the precipitates, thereby widening the lamellar structure of the eutectic phase. In addition, more porosity was observed in the HPDC alloy (marked by arrows in Fig. 3(b)) and it was not significant in the IC alloy. The higher porosity observed in the HPDC alloy was attributed to the difference in liquid metal temperature (i.e., casting temperature), die (mold) temperature, metal injection rate into the die as well as casting conditions including the process of melt preparation and the possibility of air entrainment during metal injection into the die [24].

In addition, the distinct difference in the solidification pressure between the two casting technologies employed in the present investigation might also influenced the microstructures of both the alloys. The higher solidification pressure in HPDC alloy might resulted in smaller grain size as well as finer second phase as compared to that of the IC alloy.

3.2 Nature of creep behaviour

The typical creep curves (strain vs. time) of the MRI230D alloy in both casting conditions tested at 70 MPa stress and at temperatures of 175°C and 200°C is shown in Fig. 4. It is evident from the figure that the differential cooling rates corresponding to the alloys produced by IC and HPDC resulted in varied creep characteristics. All the curves exhibited a distinct primary (transient) creep regime followed by a steady state (secondary) creep. All the creep tests were conducted under compression and therefore, the tertiary stage is not observed in the plots. The creep rate (strain rate) was calculated from the steady state region of the strain vs. time curves for all the specimens i.e., from the second stage in each case. The calculation of strain rate values based on the linear fit in the steady state region of the creep plots in Fig. 4 is shown in Fig. 5. The HPDC alloy exhibited a creep rate of 1.74×10^{-8} s^{-1} at 175°C and it was enhanced to 5.35×10^{-8} s^{-1} at 200°C i.e., the creep rate has increased by a factor of 3.1. Similarly, the IC alloy exhibited a creep rate of 3.92×10^{-8} s^{-1} at 175°C and it was enhanced to 1.28×10^{-7} s^{-1} at 200°C i.e., the creep rate has increased by a factor of 3.3. It is obvious that the increase in creep rate is more significant for the IC alloy as compared to the HPDC alloy when the temperature is raised from 175°C to 200°C. Evidently, higher creep rates were exhibited by the IC alloy as compared to the HPDC alloy at all the stress levels and temperatures employed in the present investigation. For example, at the stress level of 70 MPa and temperature of 175°C, the IC and HPDC alloys exhibited creep rates of 3.92×10^{-8} s^{-1} and 1.74×10^{-8} s^{-1}, respectively and therefore, the creep rates vary by a factor of 2.25.

Similarly, at the stress level of 70 MPa and temperature of 200°C, the IC and HPDC alloys exhibited creep rates of 1.28×10^{-7} s^{-1} and 5.35×10^{-8} s^{-1}, respectively and therefore, the creep rates vary by a factor of 2.35. The observed creep rates were differed only by a factor and not even by an order. Thus, the difference in creep rates in the MRI230D alloy in two different casting conditions was not very significant. The present observation urged us to include the reproducibility of the creep results carried out on the HPDC alloy at a stress level of 70 MPa and temperature of 200°C and the plots are shown in Fig. 6(a). The creep rate calculated from the linear fit corresponding to Fig. 6(a) is shown in Fig. 6(b). The observed creep rates are 6.30×10^{-8} s^{-1}, 5.35×10^{-8} s^{-1} and 5.79×10^{-8} s^{-1} corresponding to first, second and third run, respectively. The creep rates vary by a factor from 1.1 to 1.8 with respect to each other, which is considered to be satisfactory reproducible creep results. The creep rate corresponding to 70 MPa and 200°C for the HPDC alloy obtained in the present investigation (i.e., 5.35×10^{-8} s^{-1}) matches pretty well with the creep rate (i.e., 5.30×10^{-8} s^{-1}) reported by Mondal et al. [19] on the same material under identical condition. The creep rates for IC and HPDC Mg alloys obtained from literature is summarized in Table 2. Zheng et al. [16] and Kim et al. [17] too reported inferior creep performance of the IC alloy as compared to the HPDC alloy whereas reverse trend in creep behaviour (i.e., superior creep performance of the IC alloy) was also reported by Zhu et al. [12]. In addition, the ratio of creep rates (i.e., $\acute{\varepsilon}_{IC}/\acute{\varepsilon}_{HPDC}$) in the present investigation matches pretty well with that calculated from Zheng et al. [16] and Kim et al. [17] with the exception of little higher value reported by Zhu et al. [12].

The stress dependence of the steady state creep rates at two different temperatures (i.e., 175°C and 200°C) in double logarithmic scale for the MRI230D alloy in both casting conditions is shown in Fig. 7. The values of the apparent stress exponent, n_a, were calculated

by fitting straight line to the data, at a fixed temperature, for both the alloys. The values of the apparent stress exponent, n_a, obtained in the present investigation varies from 5.1 to 5.2, which suggests the dislocation climb being the dominant creep mechanism [25-27] in the alloy in both casting conditions. The values of the apparent stress exponent, n_a, obtained in the present investigation match pretty well with that reported on the same materials by Dieringa et al. [28]. The apparent activation energy, Q_c, cannot be calculated in the present investigation owing to the limited data. Terada et al. [29] too concluded that the rate controlling mechanism in the AX52 (Mg-5Al-2Ca) alloy was dislocation creep. Dislocation climb was reported to be the dominant creep mechanism in Mg alloys [30-32].

The deformation mechanism operated in the MRI230D alloy at the stress level of 70 MPa and at the temperatures of 175°C and 200°C determined based on the experimental data was further correlated using numerical calculation. The values of normalized stress (σ/G) and homologous temperature (T/T_m) were calculated. The value of Young's modulus (E) of the alloy was considered as 45 GPa [33] and the poisson's ratio for metal was taken as 0.33 in order to obtain the value of shear modulus (G) of 32.14 GPa. Accordingly, a value of $2.18*10^{-3}$ was obtained for (σ/G), which lies in the theoretical range of dislocation creep (i.e., $10^{-4} < (\sigma/G) < 10^{-2}$) [34]. The values of ($T/T_m$) were 0.48 and 0.51 at 175°C and 200°C, respectively. The points corresponding to the values of the combinations of (σ/G) and (T/T_m) were observed to lie within the theoretical region of dislocation creep in the deformation mechanism map developed for Mg alloy [35].

3.3 Microstructural changes after creep tests

The XRD patterns obtained from the creep tested specimens of the MRI230D alloy in both casting conditions are incorporated in Fig. 1. Comparison of the patterns obtained before and

after creep tests from the alloy in both casting conditions revealed that there was no new phase formation in the alloy specimens following creep exposure. However, there is obvious increase in intensity of the peaks corresponding to the C36 phase in the creep tested specimens of the alloy in both casting conditions, which signifies that the volume fraction of the pre-existing C36 phase increased in the alloy following creep tests. The SEM micrographs of the IC and HPDC MRI230D alloys after 50 h of creep test at a stress level of 70 MPa and temperature of 200ºC is shown in Fig. 8(a&b). The only change was identified to be the nature and the amount of phase present along the grain boundaries and the triple points in the microstructures of the creep tested specimens of both alloys as compared to the as-cast microstructures. It was observed that in both IC and HPDC alloys following 50 h of creep test the amount of pre-existing C36 phase was increased, which was confirmed by the XRD patterns as well. The precipitation of eutectic C36 phase took place close to α-Mg grain boundaries where the Al supersaturation was probably more pronounced before subjecting the specimens to creep tests. The intermetallic C36 phase is thermally stable up to 500ºC (773K) owing to its higher melting point and reported to be beneficial for creep resistance [36,37], which resulted in a lower steady state strain rate in the HPDC alloy. Further, there was no evidence of formation of any new phase in the alloy in both casting conditions even after subjecting them to creep tests at 175ºC or 200ºC. Only the amount of C36 phase was increased in all the specimens after creep tests and the maximum amount was observed in the HPDC specimens, as the total amount of pre-existing C36 phase was more in it. Mondal et al. [19] too reported an increase in C36 phase only following creep tests in the MRI230D alloy. The C36 phase was transforming into C15 (Al_2Ca) phase in the Mg–5.0Al–3.0Ca (wt.%) alloy following exposure to heat at 300ºC for 100 h [38]. However, the temperature and duration employed in the present investigation are lower and therefore, there was no change observed in the C36 phase following the creep tests. The same behaviour was also observed

in the alloys following creep tests for 50 h at a stress level of 70 MPa and temperature of 175ºC.

In order to analyze the influence of porosity on the observed creep behaviour of the HPDC MRI230D alloy the optical macrograph of the HPDC alloy after creep test for 50 h at 70 MPa stress and temperature of 200°C in shown Fig. 9. The porosity present in the optical micrographs (Fig. 2(b) and Fig. 9) looks black. Comparison of the porosity observed in the optical micrographs acquired before and after creep tests from the HPDC alloy revealed that the porosities were isolated and not connected with each other in the micrograph of the as-received alloy. In contrast, the porosities in the HPDC alloy were connected with each other and formed cracks (marked by arrows in Fig. 9) during the course of creep testing. Thus, the porosity in the HPDC alloy promoted easy crack initiation and its subsequent propagation during creep test, which deteriorated its creep behaviour.

3.4. Reason for difference in creep behaviour

The as-cast microstructure is generally inhomogeneous and the conditions prevailing during casting are far away from equilibrium solidification. Thus, the difference in creep behaviour is attributed to the diverse microstructural characteristics. The dominant creep mechanism operated in the alloys employed in the present investigation is dislocation creep. Evidently, when creep deformation is controlled by dislocation movement, any obstacle to dislocation glide and/or dislocation climb on basal and/or non-basal plane in the microstructure are expected to enhance the resistance to creep deformation. The HPDC alloy with finer grain size is expected to exhibit superior room temperature mechanical properties. However, the grain size has least influence on the creep deformation while it is controlled by dislocation creep. The better creep resistance exhibited by the HPDC alloy is mainly attributed to the

presence of finer, denser network of the fine platelets of eutectic C36 phase in the α-Mg matrix present along the grain boundaries and triple points. The C36 phase is reported to be thermally stable up to 500ºC (773K) and it hindered the dislocation movement making recovery much more difficult. Accordingly, the alloy continued work hardening, which resulted in lower creep strain during creep deformation. Thus, the dispersion strengthened α-Mg matrix resulted in better creep resistance in the HPDC alloy. In contrast, the lower volume fraction of the C36 phase in IC alloy is expected to contribute less to dispersion strengthening effect. The relatively coarse eutectic phase in IC alloy is also testified to be a reason behind lower pinning effect on the dislocation movement. Zheng et al. [16] too reported that the well-dispersed precipitates have considerable ability to retard dislocation motion on basal plane. Kim et al. mentioned that coarse eutectic phase preferred to initiate cracks easily and thus, allow dislocation movement [17]. The relatively higher porosity observed in HPDC alloy attributed negatively to the creep behaviour observed in the present investigation. Gutman et al. [9,24] established that in the case of HPDC alloy, the magnitude of creep is defined by the extent of micro and macro porosity in the alloy. They experimentally observed that under identical test conditions the minimum creep rate significantly increases with increase in porosity. However, the adverse effect of the presence of porosity in the creep behaviour of the HPDC alloy in the present investigation was counter balanced by the others factors contributing favourably towards better creep resistance.

Another plausible cause behind the difference in creep behaviour in the alloy in two different casting conditions could be the resistance to dislocation motion in the α-Mg by the presence of solute elements and/or precipitates in the grain interiors that were partitioned during solidification or formed during the course of creep exposure. The partitioning of elements to the α-Mg phase in MRI230D alloy was measured by an electron microprobe segregation

mapping by Terbush et al. [39]. They reported that the differences in the partitioning of Al and Ca to the α-Mg phase during solidification influenced both solid solution strengthening and precipitation hardening, which enhanced creep resistance in the alloy. Recent investigations [40-43] revealed that thermally stable fine precipitates in the α-Mg phase increased creep resistance of alloy. Suzuki et al. [40] reported an increase in creep resistance by a factor of 1.5-2 in die-cast and aged AXJ530 alloy causing precipitation of Al_2Ca phase on basal planes. Using TEM they concluded that the precipitates were effective obstacles against dislocation motion. Backes et al. [44] observed precipitates with an average size of 50 nm in the grain interiors of the MRI230D alloy after creep deformation, which exhibited superior creep resistance in the alloy. Amberger et al. [45] too reported the improved creep resistance by precipitation hardening caused by the presence of fine precipitates in the α-Mg phase in MRI230D alloy.

4. Conclusions

The relationship between the as-cast microstructure and creep behaviour of the MRI230D Mg alloy fabricated by two different casting technologies (i.e., ingot-casting (IC) and high pressure die-casting (HPDC)) were examined. Following are the conclusions arising out of the present investigation.

1. The HPDC alloy exhibited relatively finer grain size, finer and denser network of the eutectic C36 phase of larger volume fraction as compared to that of the IC alloy. The extent of porosity was higher in the HPDC alloy as well.
2. Superior creep resistance was exhibited by the HPDC alloy than the IC alloy at all the stress levels and temperatures employed in the present investigation.
3. The better creep resistance of the HPDC alloy was mainly attributed to the finer and denser network of higher volume fraction of the eutectic C36 phase present along the

grain boundaries and triple points in α-Mg matrix hindering dislocation movement during creep deformation.

4. The amount of eutectic C36 phase was enhanced in both alloys following creep tests and it was higher in the HPDC alloy, which is beneficial for creep resistance.

References

[1] G.V. Raynor, The Physical Metallurgy of Magnesium and Its Alloys, Pergamon Press, London-New York-Paris-Los Angeles, 1959.

[2] M.S. Dargusch, G.L. Dunlop, K. Pettersen, in: B.L. Mordike, K.U. Kainer (Eds.), Magnesium Alloys and Their Applications, Werkstoff-Informationsgesellschaft, Frankfurt, 1998, pp. 277-282.

[3] A.A. Luo, Int. Mater. Rev. 49 (2004) 13-30.

[4] M.O. Pekguleryuz, A.A. Kaya, Adv. Eng. Mater. 5 (2004) 866-878.

[5] B.C. Pai, U.T.S. Pillai, A. Srinivasan, Indian Foundry J. 57 (2011) 35-43.

[6] Q.D. Wang, W.Z. Chen, X.Q. Zeng, Y.Z. Lu, W.J. Ding, Y.P. Zhu, X.P. Xu, J. Mater. Sci. 36 (2001) 3035-3040.

[7] S.S. Li, B. Tang, D.B. Zeng, J. Alloys Compd. 437 (2007) 317-321.

[8] E. Aghion, B. Bronfin, F.V. Buch, S. Schumann, H. Friedrich, JOM 55 (2003) 30-33.

[9] E.M. Gutman, Ya. Unigovski, M. Levkovich, Z. Koren , E. Aghion, M. Dangur, Mater. Sci. Eng. A 234-236 (1997) 880-883.

[10] S. Spigarelli, M. Regev, E. Evangelista, A. Rosen, Mater. Sci. Tech. 17 (2001) 627-638.

[11] C.H. Caceres, C.J. Davidson, J.R. Griffiths, C.L. Newton, Mater. Sci. Eng. A 325 (2002) 344-355.

[12] S.M. Zhu, B.L. Mordike, J.F. Nie, Mater. Sci. Eng. A 483-484 (2008) 583-586.

[13] L. Han, D.O. Northwood, X. Nie, H. Hu, Mater. Sci. Eng. A 512 (2009) 58-66.

[14] A. Srinivasan, J. Swaminathan, M.K. Gunjan, U.T.S. Pillai, B.C. Pai, Mater. Sci. Eng. A 527 (2010) 1395-1403.

[15] T.V. Ferri, A.P. Figueiredo, C.R.F. Ferreira, W. Hormaza, C.A. Santos, J.A. Spim, Mater. Sci. Eng. A 527 (2010) 4624-4632.

[16] J. Zheng, Q. Wang, Z. Jin, T. Peng, J. Alloys Compd. 496 (2010) 351-356.

[17] B.H. Kim, S.M. Jo, Y.C. Lee, Y.H. Park, I.M. Park, Mater. Sci. Eng. A 535 (2012) 40-47.

[18] J. Bai, Y. Sun, F. Xue, J. Qiang, Mater. Sci. Eng. A 552 (2012) 472-480.

[19] A.K. Mondal, D. Fechner, S. Kumar, H. Dieringa, P. Maier, K.U. Kainer, Mater. Sci. Eng. A 527 (2010) 2289-2296.

[20] Y. Terada, R. Sata, N. Ishimatsu, T. Sato, K. Ohori, Metall. Mater. Trans. A 35 (2004) 3029-3032.

[21] S.W. Xu, K. Oh-ishi, S. Kamado, F. Uchida, T. Homma, K. Hono, Scripta Mater. 65 (2011) 269-272.

[22] E.J. Lavernia, T.S. Srivatsan, J. Mater. Sci. 45 (2010) 287-325.

[23] A. Finkel, M. Regev, E. Aghion, M. Bamberger, A. Rosen, in: E. Aghion, D. Eliezer (Eds.), Proceedings of the First Israel International Conference on Magnesium Science and Technology, Magnesium Research Institute, Beer-Sheva, Israel, 1997, pp. 121-126.

[24] E.M. Gutman, Y. Unigovski, M. Levkovitch, Z. Koren, J. Mater. Sci. Lett. 17 (1998) 1787-1789.

[25] O.D. Sherby, P.M. Burke, Prog. Mater. Sci. 13 (1968) 325-390.

[26] F.A. Mohamed, T.G. Langdon, Acta. Metall. (1974) 22(6) 779-788.

[27] J. Weertman, J. Appl. Phys. 28 (1957) 1185-1189.

[28] H. Dieringa, Y. Huang, P. Wittke, M. Klein, F. Walther, M. Dikovits, C. Poletti, Mater. Sci. Eng. A 585 (2013) 430-438

[29] Y. Terada, N. Ishimatsu, T. Sato, Mater. Trans. 48 (2007) 2329-2335.

[30] A. Arunachaleswaran, I.M. Pereira, H. Dieringa, Y. Huang, N. Hort, B.K. Dhindaw, Mater. Sci. Eng. A 460–461 (2007) 268-76.

[31] H. Dieringa, Y. Huang, P. Mainer, N. Hort, K.U. Kainer, Mater. Sci. Eng. A 410-411 (2005) 85-89.

[32] V. Sklenicka, T.G. Langdon, J. Mater. Sci. 39 (2004) 1647-1652

[33] http://www.dsm.co.il, Last accessed on 28 October 2014.

[34] G.E. Dieter, Mechanical Metallurgy, fourth ed., McGraw-Hill, London, 2000.

[35] H.J. Frost, M.F. Ashby, Deformation-Mechanism Maps, The Plasticity and Creep of Metals and Ceramics, Pergamon Press, Oxford, UK, 1982.

[36] A.A. Luo, M.P. Balogh, B.R. Powell, Metall. Mater. Trans. A 33 (2002) 567-573.

[37] A. Suzuki, N.D. Saddock, J.W. Jones, T.M. Pollock, Metall. Mater. Trans. A 37 (2006) 975-983.

[38] A. Suzuki, N.D. Saddock, J.W. Jones, T.M. Pollock, Acta Mater. 53 (2005) 2823-2834.

[39] J.R. Terbush, N.D. Saddock, J.W. Jones, T.M. Pollock, Metal. Mater. Trans. A 41 (2010) 2435-2442.

[40] A. Suzuki, N.D. Saddock, J.R. TerBush, B.R. Powell, J.W. Jones, T.M. Pollock, in: R.S. Beals, A.A. Luo, N.R. Neelameggham, M.O. Pekguleryuz (Eds.), Magnesium Technology 2007, TMS, Warrendale, PA, 2007, pp. 375-380.

[41] X. Gao, S.M. Zhu, B.C. Muddle, J.F. Nie, Scripta Mater. 53 (2005) 1321-1326.

[42] J.F. Nie, X. Gao, S.M. Zhu, Scripta Mater. 53 (2005) 1049-1053.

[43] M. Vogel, O. Kraft, E. Arzt, Scripta Mater. 48 (2003) 985-990.

[44] B. Backes, K. Durst, D. Amberger, M. Göken, Metal. Mater. Trans. A 40 (2009) 257-261.

[45] D. Amberger, P. Eisenlohr, M. Göken, Acta Mater. 60 (2012) 2277-2289.

Figure captions

Fig. 1. XRD patterns for the MRI230D alloys in two different casting conditions.

Fig. 2. Optical micrographs of the MRI230D alloy in (a) IC and (b) HPDC conditions.

Fig. 3. SEM micrographs of the MRI230D alloy in (a) IC, (b) HPDC conditions and (c) magnified view of (b).

Fig. 4. Strain vs. time plots for the IC and HPDC MRI230D alloys creep tested for 50 h at 70 MPa stress and temperatures of 175°C and 200°C.

Fig. 5. Calculation of strain rates by linear fit to the strain vs. time plots shown in Fig. 4.

Fig. 6.(a) Strain vs. time plots corresponding to three different runs and (b) calculation of strain rates by linear fit to the plots shown in (a) for the HPDC MRI230D alloy tested for 50 h at 70 MPa stress and temperature of 200°C.

Fig.7. The stress dependence of steady state creep rate for HPDC MRI230D alloy.

Fig. 8. SEM micrographs of the MRI230D alloys after creep test for 50 h at 70 MPa stress and temperature of 200°C in (a) IC and (b) HPDC conditions.

Fig. 9. Optical micrograph of the HPDC MRI230D alloy after creep test for 50 h at 70 MPa stress and temperature of 200°C.

Table

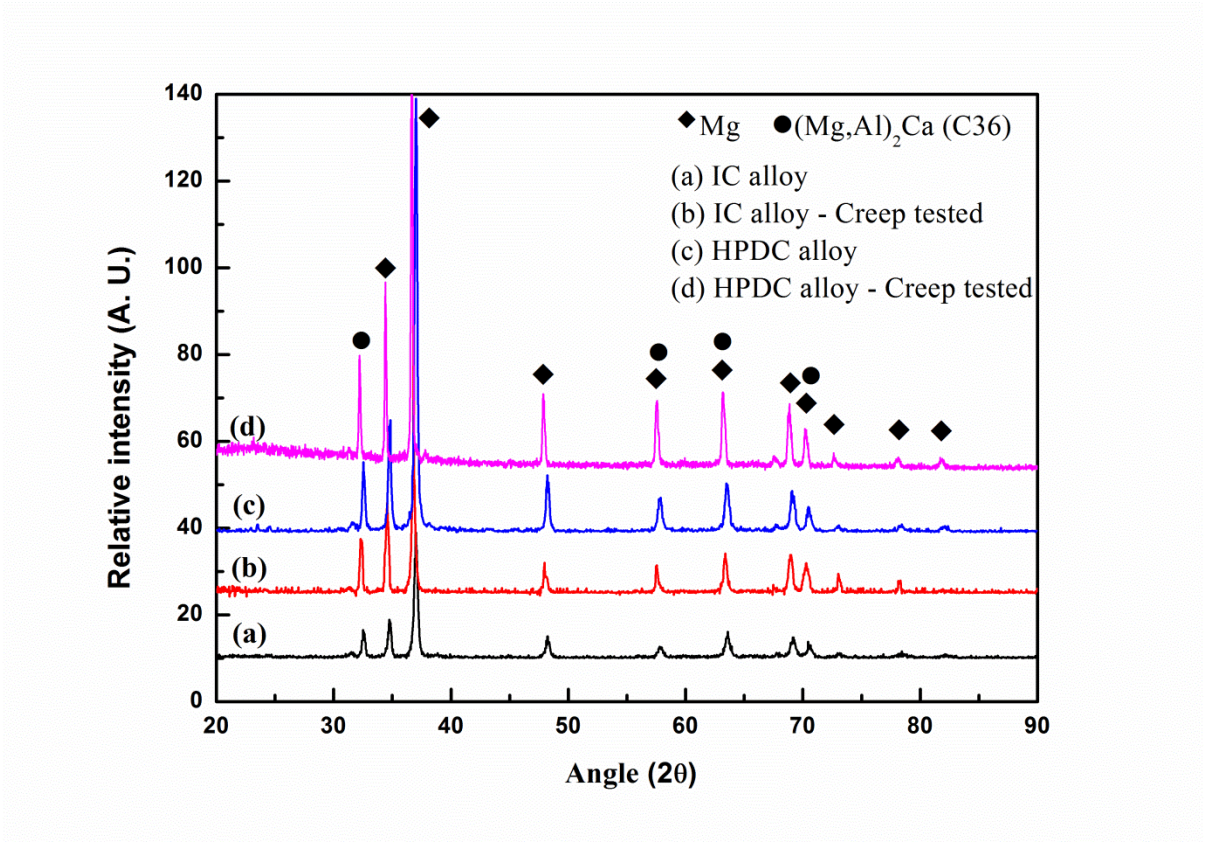

Fig. 1. XRD patterns for the MRI230D alloys in two different casting conditions.

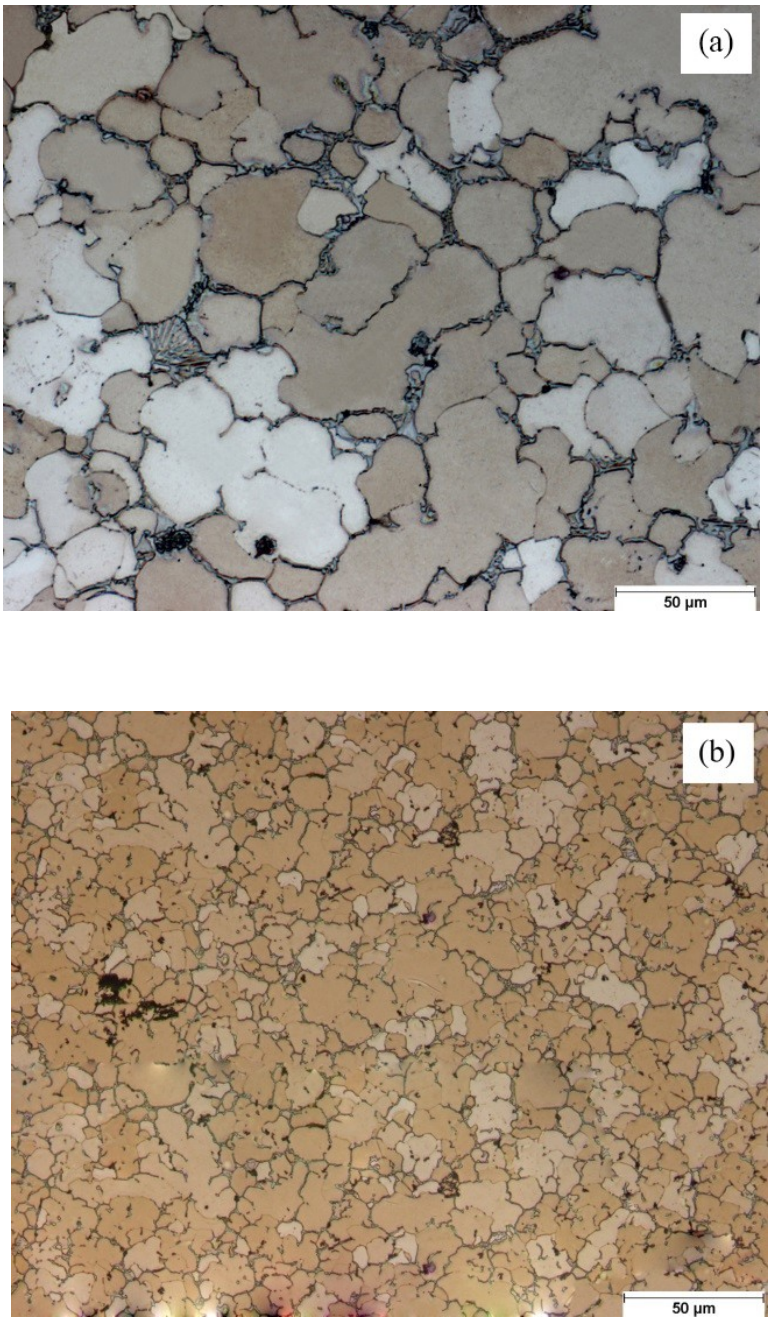

Fig. 2. Optical micrographs of the MRI230D alloy in (a) IC and (b) HPDC conditions.

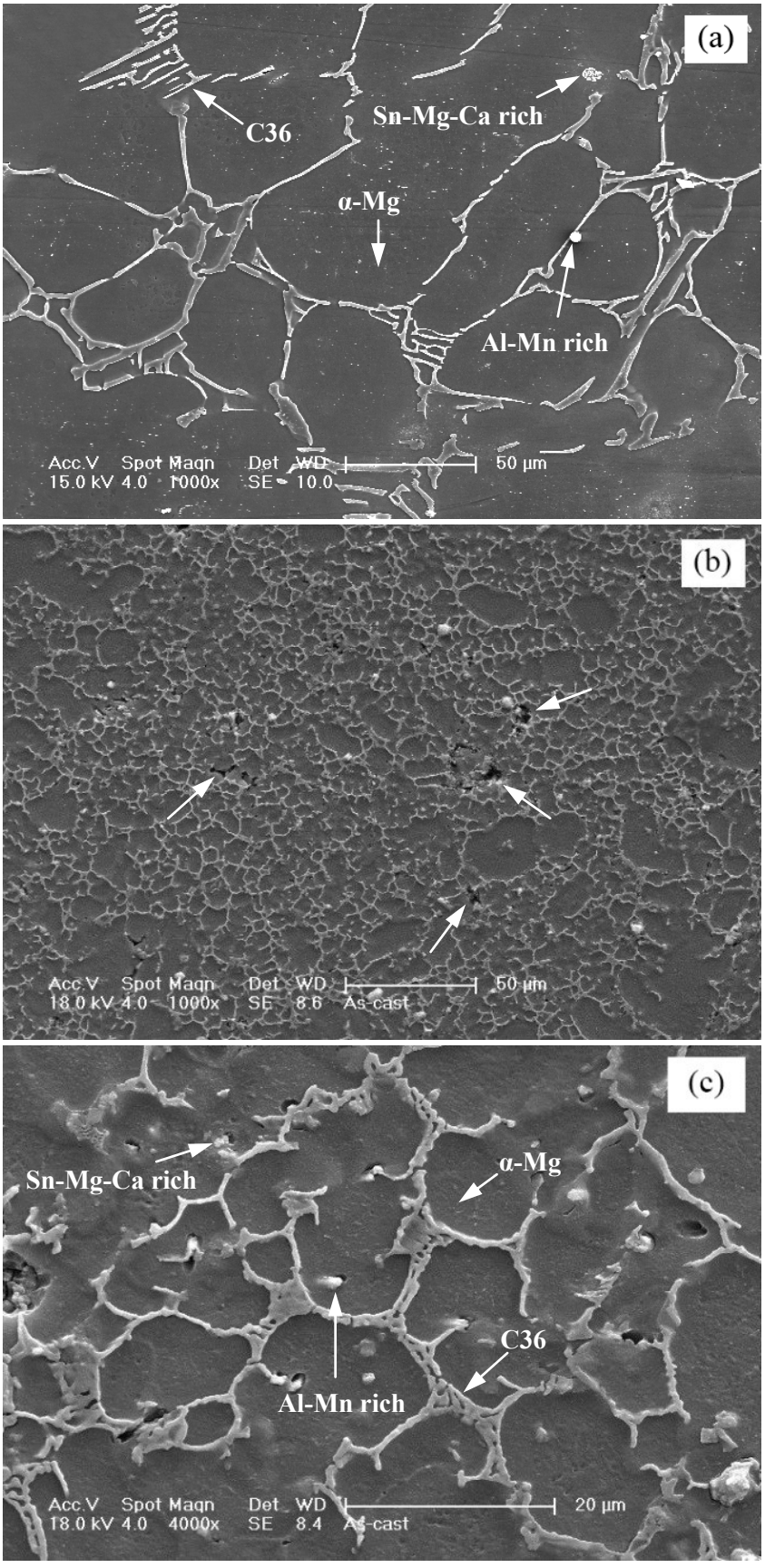

Fig. 3. SEM micrographs of the MRI230D alloy in (a) IC, (b) HPDC condiitions and (c) magnified view of (b).

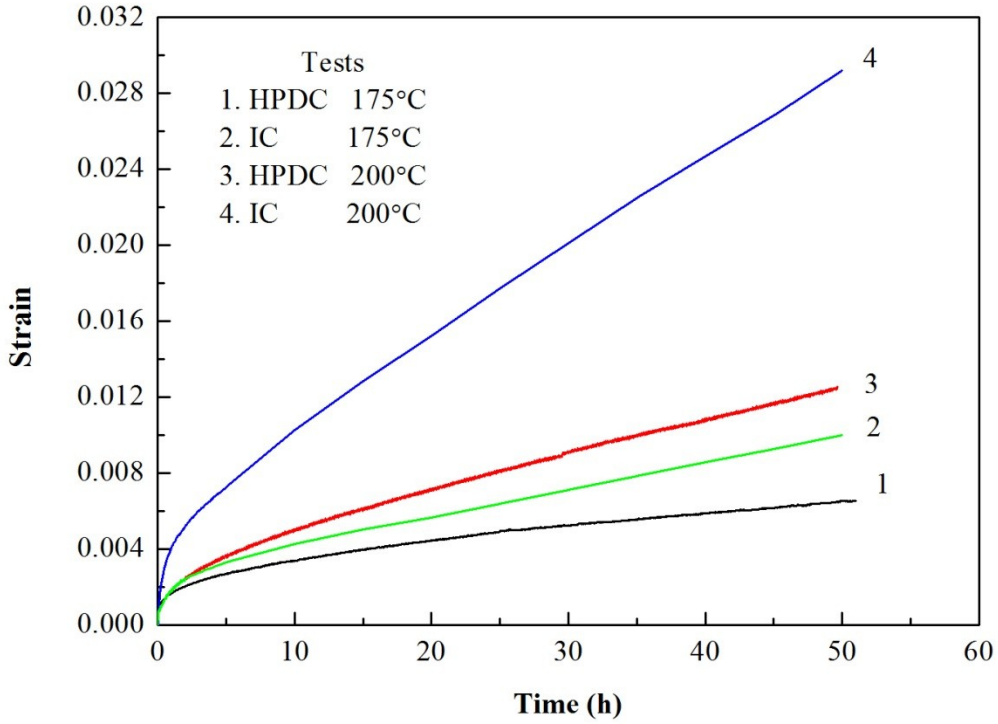

Fig. 4. Strain vs. time plots for the IC and HPDC MRI230D alloys creep tested for 50 h at 70 MPa stress and temperatures of 175°C and 200°C.

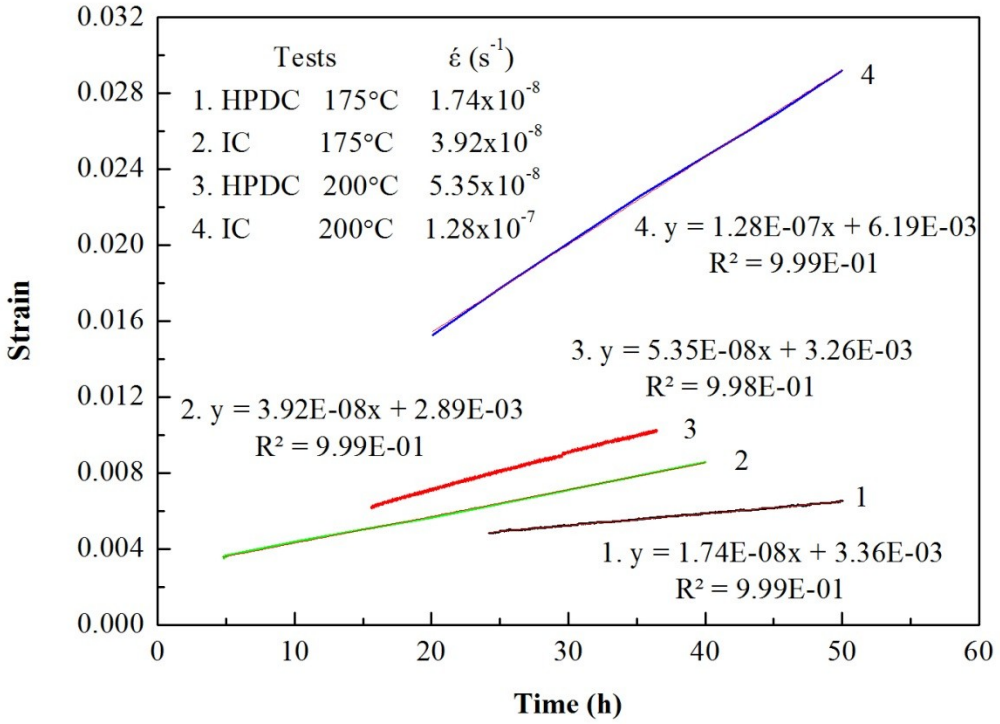

Fig. 5. Calculation of strain rates by linear fit to the strain vs. time plots shown in Fig. 4.

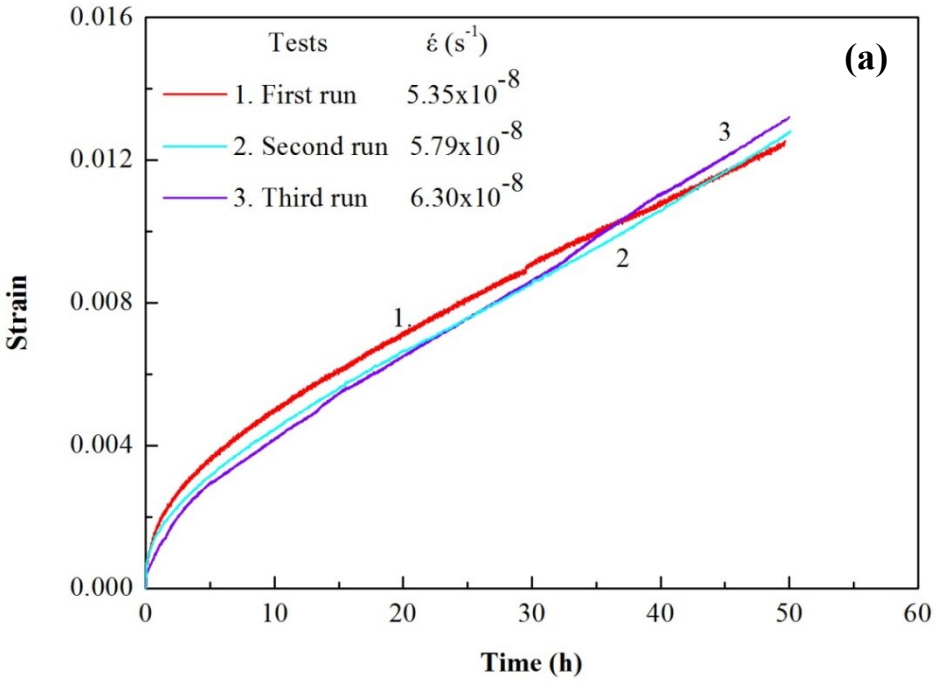

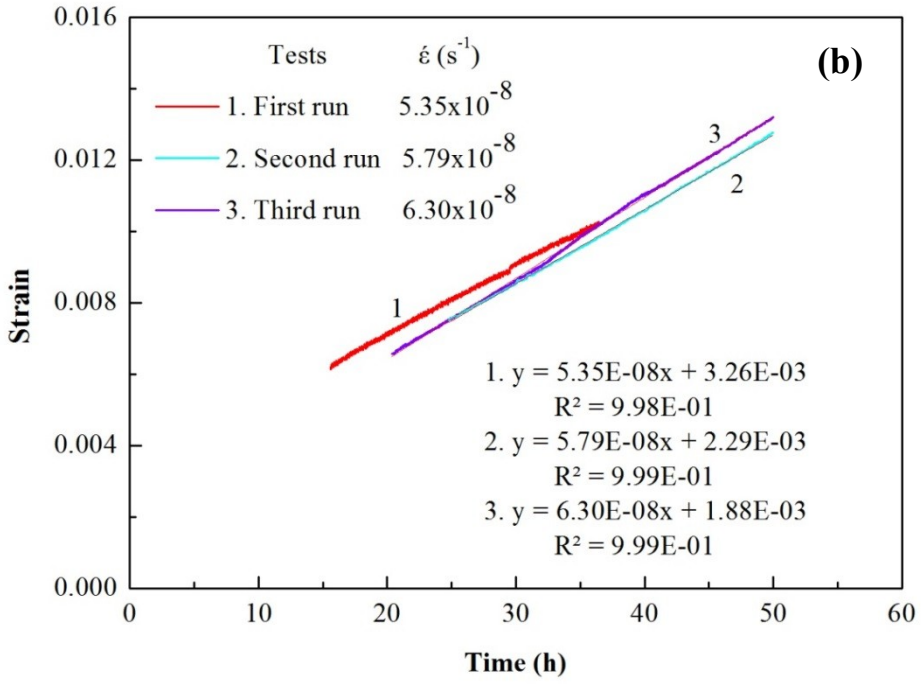

Fig. 6.(a) Strain vs. time plots corresponding to three different runs and (b) calculation of strain rates by linear fit to the plots shown in (a) for the HPDC MRI230D alloy tested for 50 h at 70 MPa stress and temperature of 200°C.

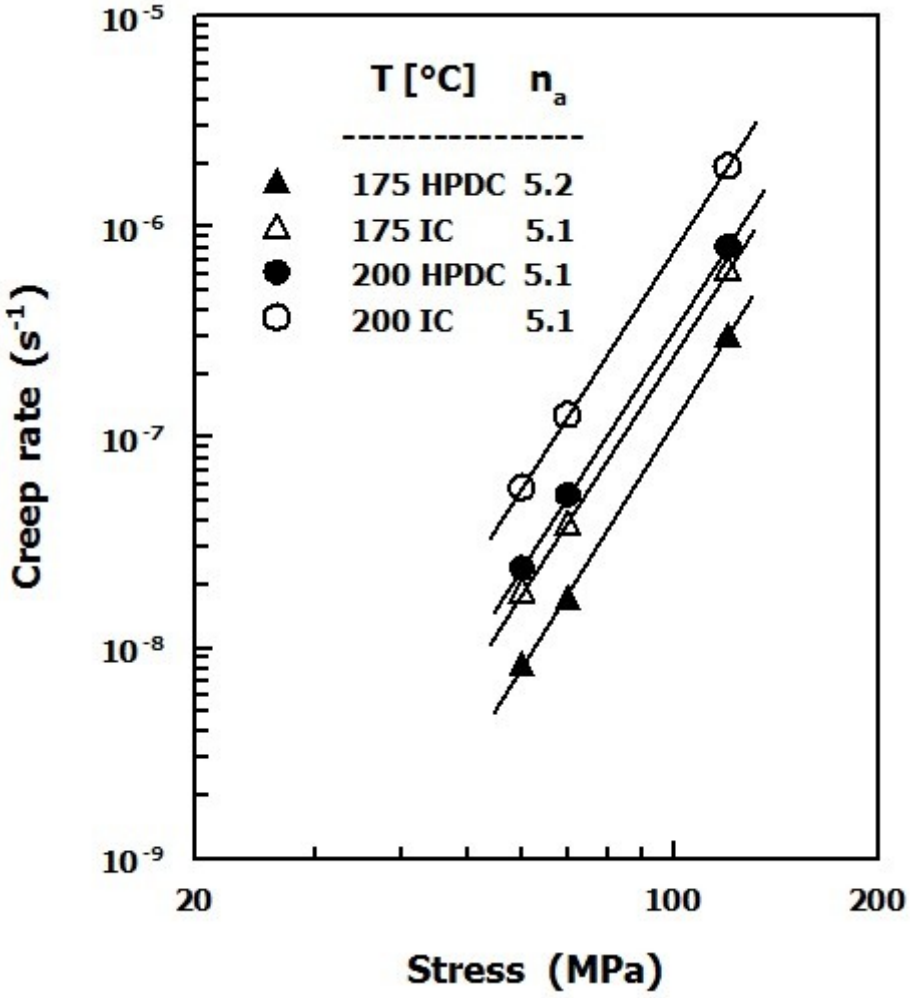

Fig.7. The stress dependence of steady state creep rate for HPDC MRI230D alloy.

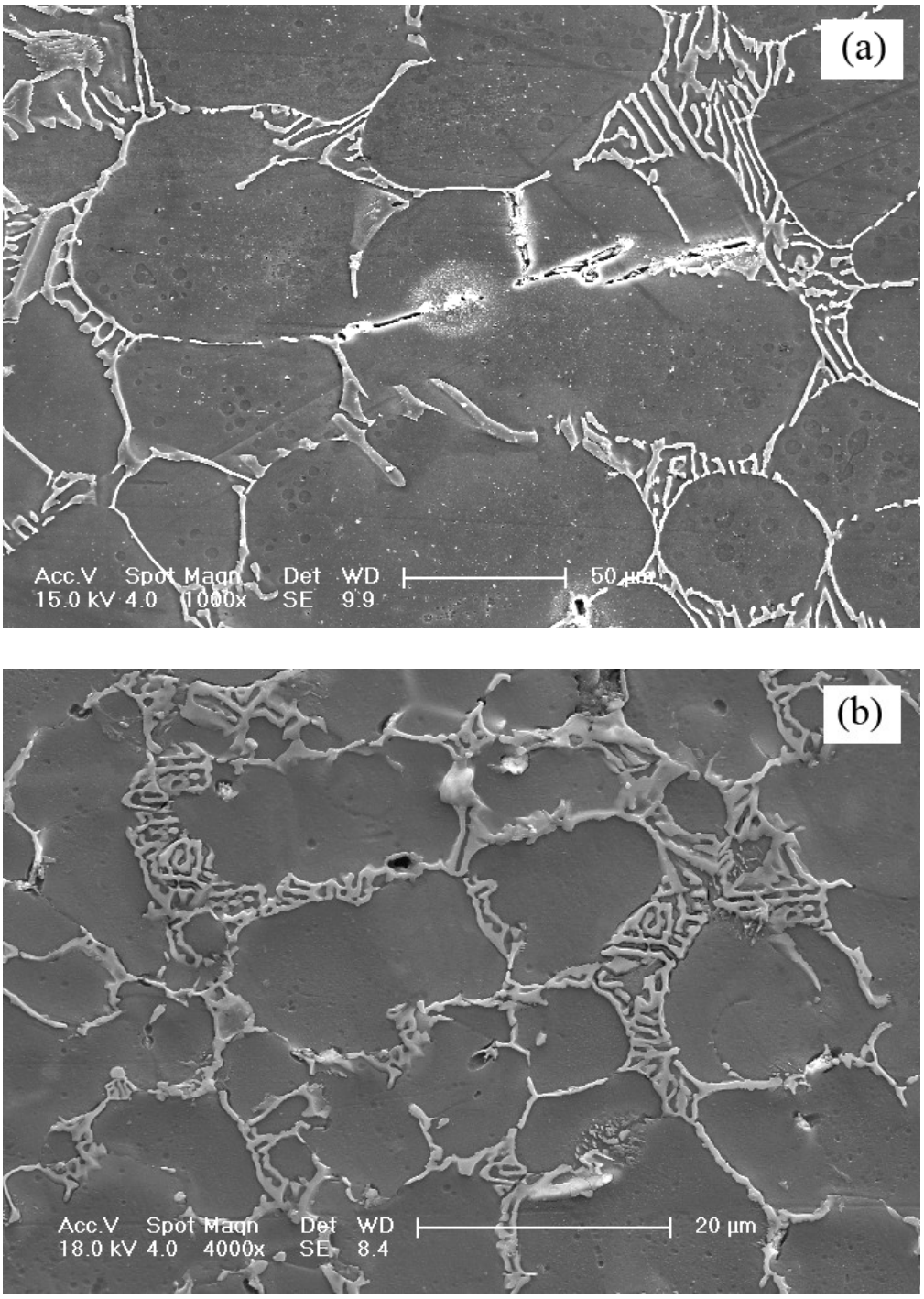

Fig. 8. SEM micrographs of the MRI230D alloys after creep test for 50 h at 70 MPa stress and temperature of 200°C corresponding to (a) IC alloy and (b) HPDC alloy.

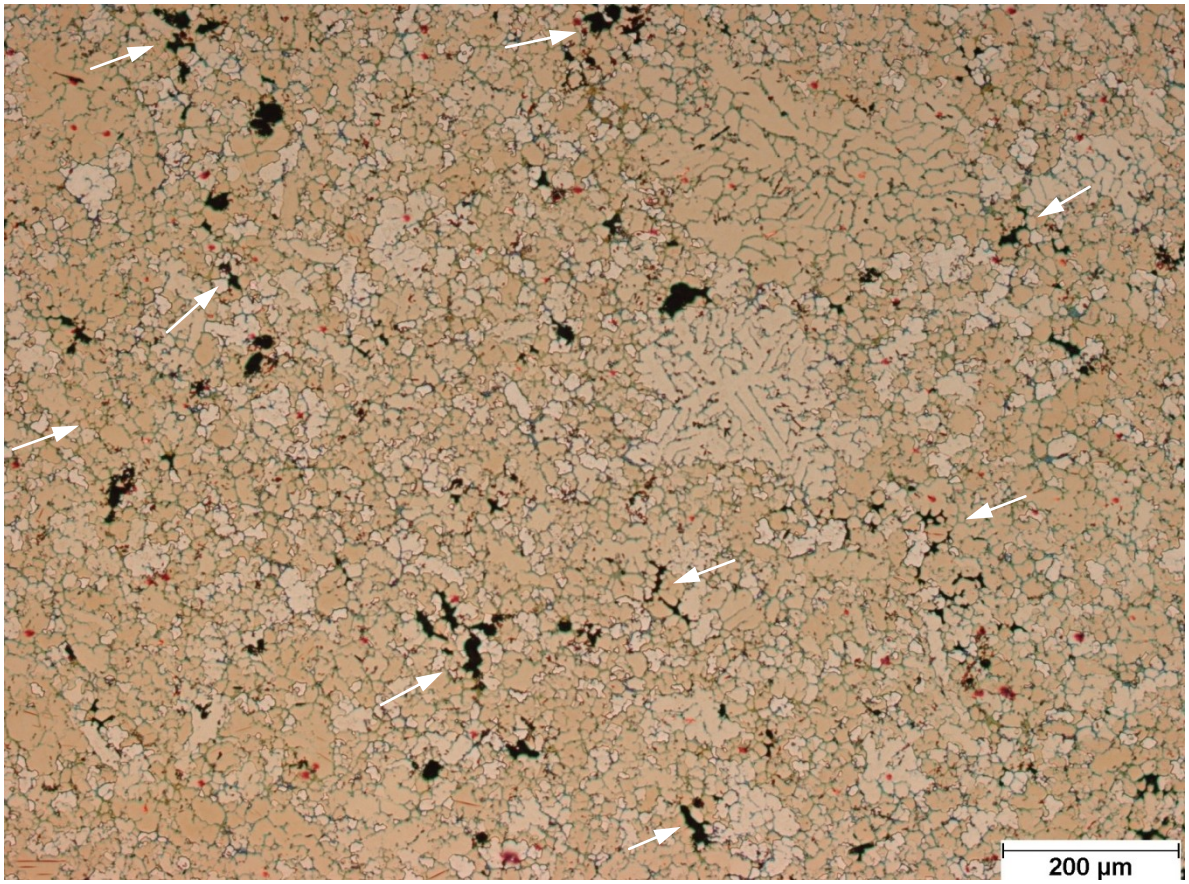

Fig. 9. Optical micrograph of the HPDC MRI230D alloy after creep test for 50 h at 70 MPa stress and temperature of 200°C.

Table 1. Nominal chemical composition of the MRI230D alloy.

MRI230D alloy	Al	Ca	Zn	Mn	Sr	Sn	Mg
Element (wt.%)	6.45	2.25	< 0.01	0.27	0.25	0.84	Balance

Table 2. Summary of creep rates for IC and HPDC Mg alloys obtained from literature.

Source	Test parameters [Temp. (T)°C; Stress (σ) MPa]	Alloy under investigation	Creep rate in IC	Creep rate in HPDC	Ratio of creep rates ($\acute{\varepsilon}_{IC}/\acute{\varepsilon}_{HPDC}$)	Remark
Zhu et al. [18]	T=150; σ=90	MRI153 (8.0Al-1.0Ca-0.6 Zn-0.3Mn-0.1Sr)	$1.0*10^{-9}$	$8.0*10^{-9}$	0.13	IC alloy is better
Zheng et al. [22]	T=200; σ=60	Mg-3.0Sm-0.5Zn-0.4Zr	$1.5*10^{-9}$	$7.0*10^{-10}$	2.14	HPDC alloy is better
Kim et al. [23]	T=150; σ =70	ATX421 (Mg-4.0Al-2.0Sn-1.0Ca)	$2.4*10^{-8}$	$7.4*10^{-9}$	3.24	HPDC alloy is better
Present study	T=175; σ =70	MRI230D (6.45Al-2.25Ca-<0.01 Zn-0.27Mn-0.25Sr-0.85Sn)	$3.92*10^{-8}$	$1.74*10^{-8}$	2.25	HPDC alloy is better
Present study	T=200; σ =70	-Do-	$1.28*10^{-7}$	$5.35*10^{-8}$	2.35	HPDC alloy is better